Supplementary Information

Sub-cellular population imaging tools reveal stable apical dendrites in hippocampal area CA3

Jason J. Moore*, Shannon K. Rashid, Emmett Bicker, Cara D. Johnson, Naomi Codrington, Dmitri B. Chklovskii, and Jayeeta Basu*

Emails of corresponding authors:
Jason.Moore@nyulangone.org
Jayeeta.Basu@nyulangone.org

This PDF file includes:

1. Supplementary Figures 1 to 18
2. Supplementary Tables 1 to 10

Supplementary Figures

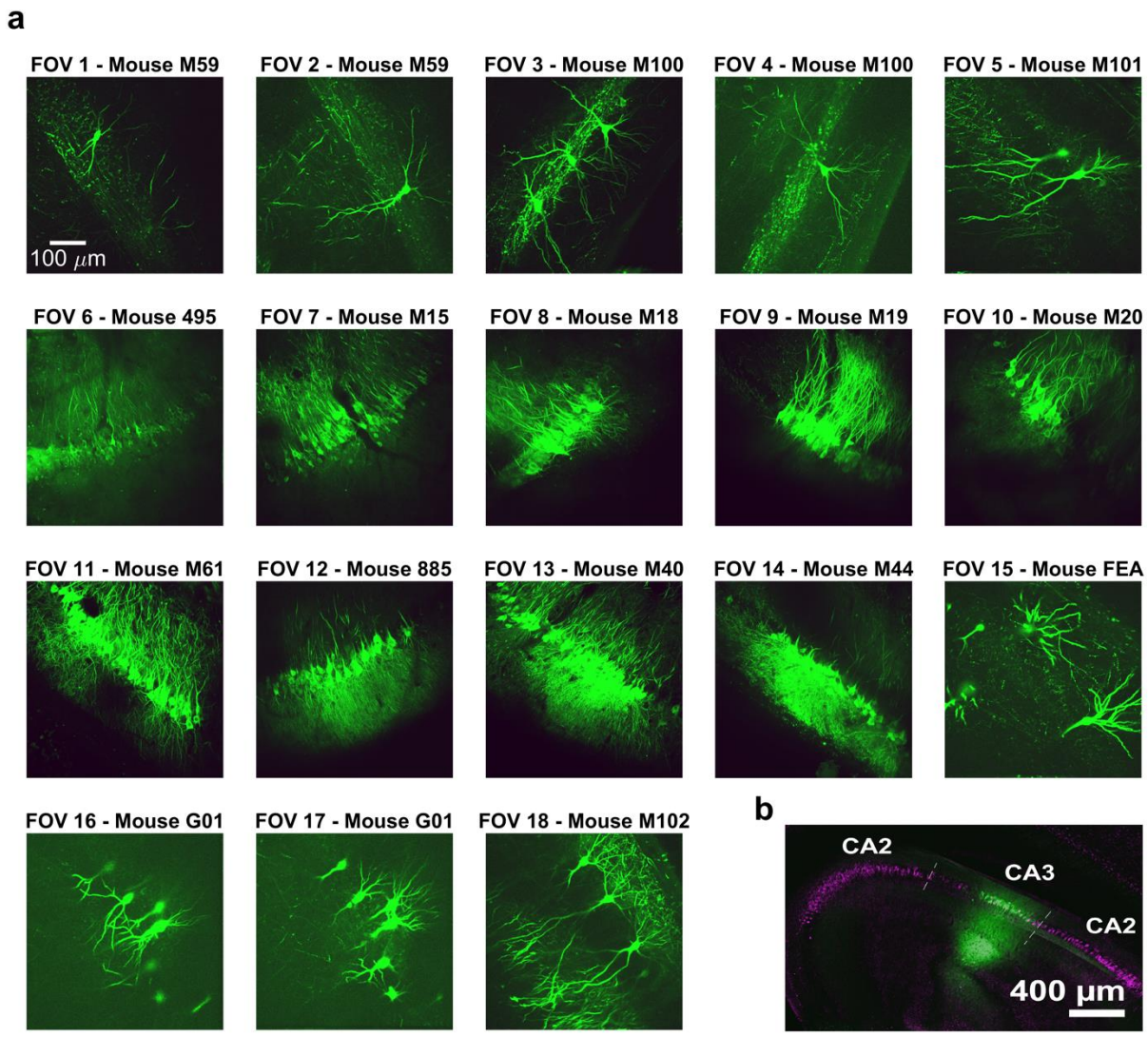

Supplementary Fig. 1 | All fields of view. a, Maximum intensity projections of all fields of view used in the study. Fields of view are annotated with the mouse identification number each field of view was recorded from, as well as viral injection details for each. FOVs 7 and 11 were used in Fig. 1c; FOV 2 was used in Fig. 1d; FOV 9 was used in Fig. 1e, Supplementary Fig. 3, and Movie 1. FOVs 1-18 were used in Fig. 1f. FOVs 1, 2, and 6-14 were used in Figs. 2, 4 and Supplementary Figs. 4, 7, and 12. FOVs 6-14 were used in Fig. 5 and Supplementary Fig. 13. FOVs 7-14 were used in Figs. 6-8 and Supplementary Figs. 6, 12, 14-15 and 17-18. FOVs 3 and 15-18 were used in the Sparse Data analyses in Supplementary Fig. 16. **b**, Representative horizontal slice showing GCaMP6f (green) is expressed in area CA3, not CA2, marked by PCP4 (pseudo-colored magenta).

Injections presented as Virus (Titer)

FOV	**GCaMP Virus**	**CaMKII Virus**	**Sex**
FOV 1-2	AAV2.1-Syn-FLEX-GCaMP6f ($8.2x10^{12}$)	AAV2.1-CaMKII-Cre ($1.36x10^{8}$)	F
FOV 3-5	AAV2.1-Syn-FLEX-jGCaMP7b ($1.64x10^{12}$)	AAV2.1-CaMKII-Cre ($2.44x10^{9}$)	M
FOV 6	Transgenic GCaMP, GP5.5, no virus	N/A	F
FOV 7-12	AAV2.1-CaMKII-GCaMP6f ($2.76x10^{13}$)	N/A	M
FOV 13-14	AAV2.1-CaMKII-GCaMP6f ($2.76x10^{13}$)	N/A	F
FOV 15	AAV2.1-Syn-FLEX-jGCaMP7b ($1.64x10^{12}$)	AAV2.1-CaMKII-Cre ($2.44x10^{9}$)	M
FOV 16-17	AAV2.1-Syn-FLEX-GCaMP6f ($1.17x10^{13}$)	AAV2.1-CaMKII-Cre ($7.74x10^{8}$)	M
FOV 18	AAV2.1-Syn-FLEX-jGCaMP7b ($1.64x10^{12}$)	AAV2.1-CaMKII-Cre ($2.44x10^{9}$)	M

Supplementary Table 1 | Injection parameters and mouse sex

a) Algorithm 1: Find ROI Cores

Input: Data matrix Y ($R^{d \times d \times t}$), Activity Threshold sigma, Size Threshold sz, Overlap Threshold ov

```
Y <- ComputeDFF(Y)                          % Transform values in Y into ΔF/F units across time
sY <- sigma*median(Y,3)                     % Compute threshold values for each pixel as a constant times the median
                                            % value across time (Dimension 3)
Y <- Threshold(Y, sY)                       % Binarize Y
        Y(x,y,t) = Y(x,y,t) > sY(x,y)

PX <- 3DConnectedComponents(Y, sz)          % Find connected components in 3D with a minimum size
A <- ProjectOnto2D(PX)                      % Project components into 2D
OV = ComputeOverlaps(A)                     % Compute the overlap between all pairs of components
        OV(i,j) = M(A_i /\ A_j)/M(A_i \/ A_j) > ov   % M( ) counts the number of elements in a set
                                            % /\ is the Intersection operator; \/ is the Union operator
A0 <- MergeOverlapping(A, OV)
Return A0
```

b) Algorithm 2: CNMF

Input: Data matrix Y ($R^{d \times d \times t}$), Initial footprints A0 ($R^{d \times d \times k}$)

```
Y <- Reshape(Y, d*d, t)                     % Reshape Y
A0 <- Reshape(A0, d*d, k)                   % Reshape A0
An <- sum(A0,2) == 0                        % Define ROI from pixels not covered by any component
Af <- ones(d*d, 1)                          % Define background ROI using all pixels
A0 <- [A0 An Af]
A <- Normalize(A0)                          % All ROIs sum to 1
C <- max((A^T A + eta*I)^-1 A^T Y, 0)       % Initial estimate of temporal components
Repeat
    A <- (1- alpha)*A + alpha*max((YC^T)(CC^T + beta*1), 0)   % 1 is a matrix of all ones; α is the learning rate; 0≤α<1
    C <- (1- alpha)*C + α*max((A^T A + eta*I)^-1 A^T Y, 0)    % I is the identity matrix
Return A, C
```

c) Algorithm 3: Merging ROIs

Input: Footprints of ROIs to be merged A ($R^{d*d \times p}$), Temporal components of ROIs to be merged C ($R^{p \times t}$)

```
Cm <- max(C,2)                              % Find maximum value across time (Dimension 2)
A2 <- max(RCm)                              % Scale ROIs by maximum value and take maximum value across scaled ROIs
A_out = A2/sqrt(A^T A)                      % Normalize to have magnitude 1 (Element-wise square root)

V <- max(AC)                                % Reconstruct the video using the ROIs to be merged, taking the maximum
                                            % value across common pixels

C_out = (A_out^T A_out)^-1 A_out^T V        % Solve for the temporal components that best reconstruct the video given
                                            % the newly-merged ROI
Return A_out, C_out
```

Supplementary Table 2 | Core algorithms of d-NMF

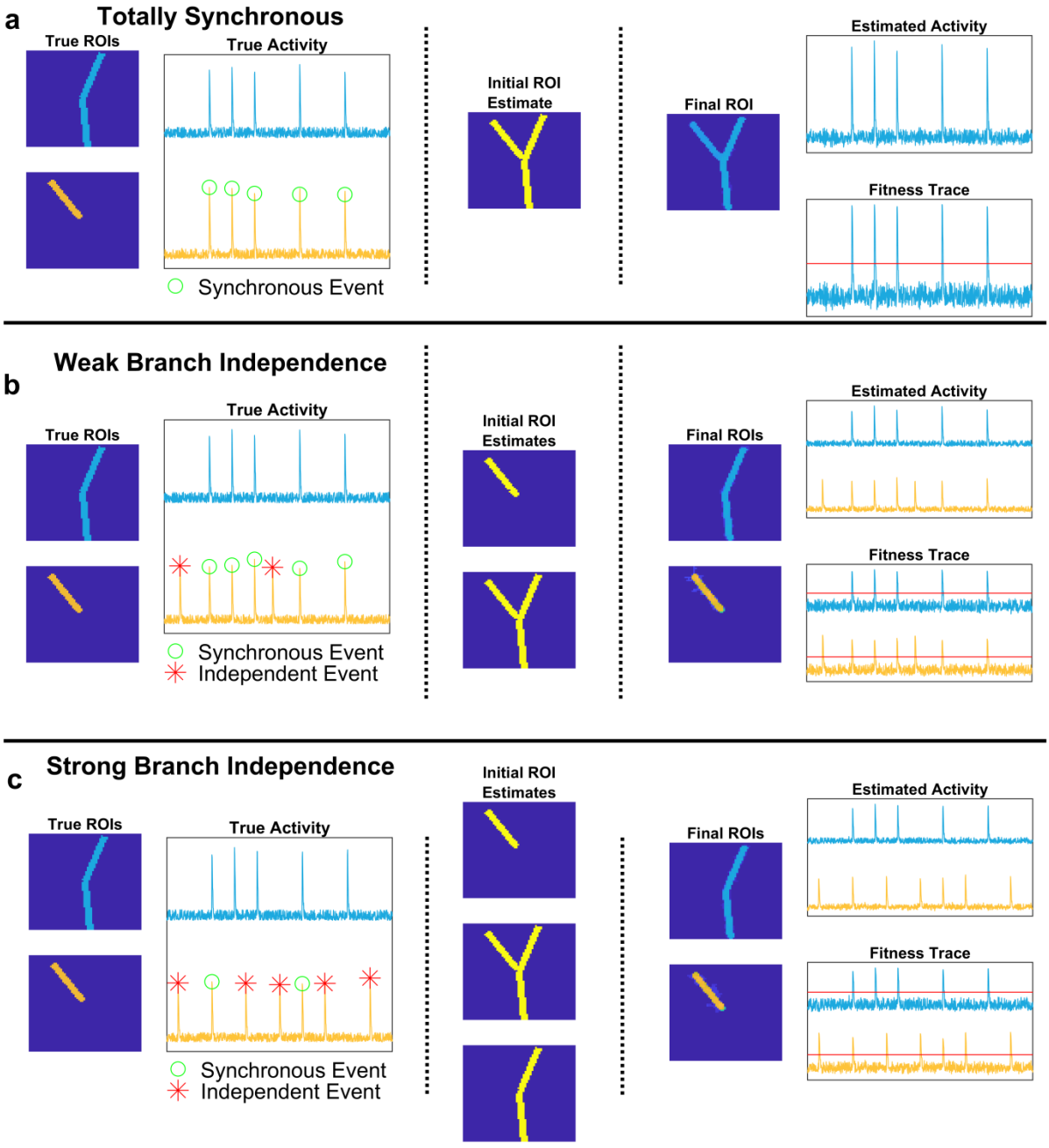

Supplementary Fig. 2 | Handling of branch-independent activity. a, Example synthetic dataset demonstrating synchronous activity within branches. Left, the true ROIs and activity are plotted. In this example, all events are synchronous between the two branches. Middle, the initial detected ROI cores estimate encompasses the entire tree. Right, after processing the estimated ROI still encompasses the entire tree, and the estimated activity is nearly identical to the true activity. All detected calcium transients cross the threshold for the fitness trace. **b**, Example situation where one branch is weakly independent from the other. Branch independent events are marked with red asterisks. The initial ROI estimates include the single branch as well as the entire tree. After the algorithm has converged, the remaining ROIs have separated the two branches and accurately estimated their activity. For both ROIs, no calcium transients are screened out by the fitness trace. **c**, Example situation where one branch is highly independent from the other two. The initial ROI estimates include the left branch, the right branch, and their union, but after processing the remaining ROIs represent the two branches separately.

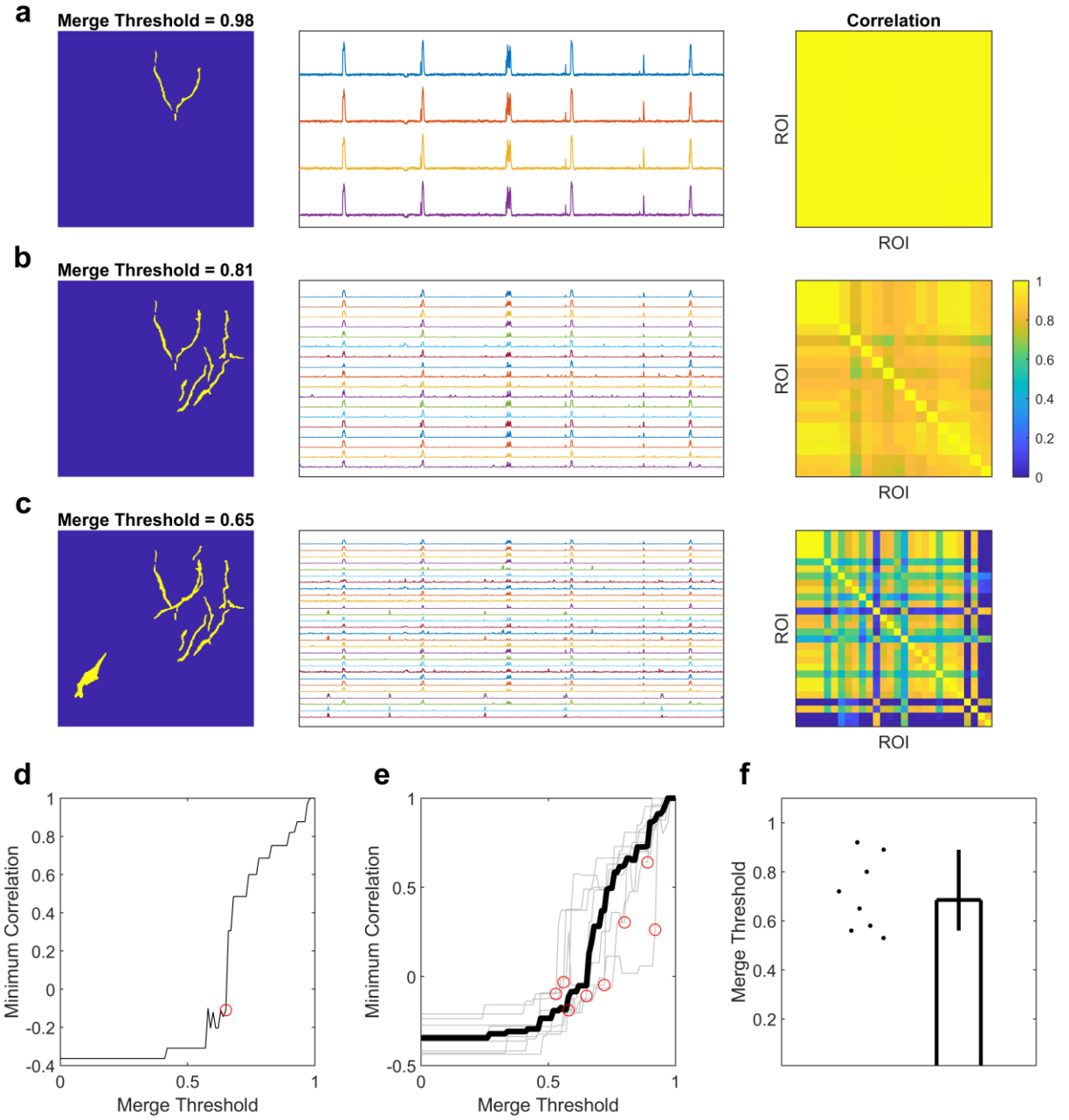

Supplementary Fig. 3 | Identifying appropriate merging thresholds. a, Left, silhouettes of ROIs belonging to a cluster based on a merging threshold of 0.98. Middle, activity traces of the corresponding ROIs, showing extremely high correlation. Right, correlation matrix of the activity traces. **b,** Same as **a** but for a merging threshold of 0.81. Note that more ROIs are added to this cluster, but their activity is all highly correlated, indicating they plausibly belong to the same neuron. **c,** Same as **a**, but for a merging threshold of 0.65. Note the addition of several ROIs with activity that is uncorrelated with most of the rest of the cluster. **d,** A plot of the minimum correlation value for the largest ROI cluster versus the merge threshold for the FOV in **a-c**. The red circle indicates the threshold at which the merging becomes too permissive (here, 0.65). **e,** Similar threshold-correlation plots for all 8 dense FOVs. The thick line indicates the median across all FOVs. **f,** The median merge threshold across all 8 dense FOVs was 0.69, [0.56, 0.89], *n* = 8 FOVs.

	CaImAn (CNMF with Sparse NMF Initialization)	suite2p	d-NMF
Initialization	• Nonnegative double singular value decomposition initialization • # of components must be specified	• Local correlations • # of components is discovered	• Local co-activity • # of components is discovered
Spatial Constraints	• None	• None	• Contiguous pixels
Temporal Constraints	• Autoregressive fit	• None	• None
ROI Selection	• Space correlation[a] • SNR • CNN classifier[b]	• Skewness • Variance • Anatomical measures[b]	• Skewness • Size • Spatial fitness[a]
Overlap	• De-mixed according to NMF	• Discard pixels belonging to multiple ROIs	• De-mixed according to NMF

Supplementary Table 3 | Comparison of method details between d-NMF, CaImAn, and suite2p

[a]The space correlation metric described in the CaImAn paper is similar to the Fitness trace measure used in this manuscript

[b]The CNN classifier described in the CaImAn paper classified ROIs as having a soma-like shape, with a similar goal as the anatomical measures described in the suite2p pre-print.

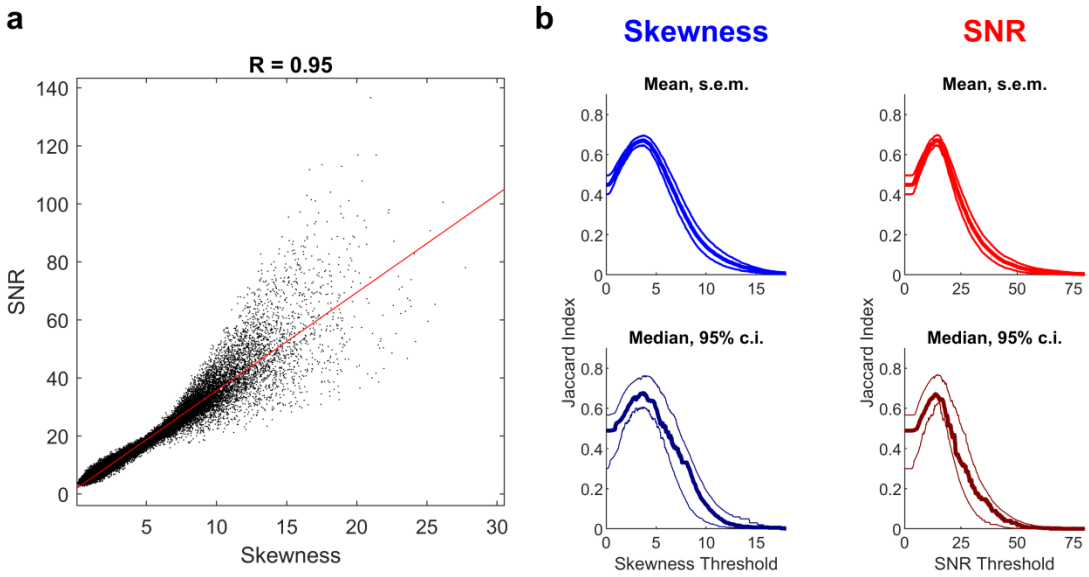

Supplementary Fig. 4 | Skewness versus signal-to-noise ratio for ROI classification. a, Skewness is strongly correlated with signal-to-noise ratio (SNR), another measure of the quality of calcium traces (R=0.95, p=0, two-sided t-test, *n* = 29,566 calcium traces from 11 fields of view from 10 mice). **b**, Overall performance of identifying true or false ROIs was similar when using Skewness (left, blue) or SNR (right, red). Peak +/- s.e.m. of mean Skewness: 0.67+/-0.02; Peak, 95% confidence interval of median Skewness: 0.68, [0.61, 0.76]; Peak +/- s.e.m. of mean SNR: 0.67 +/-0.03; Peak, 95% confidence interval of median SNR: 0.67, [0.62, 0.76]). *n* = 11 FOVs for panel **b**.

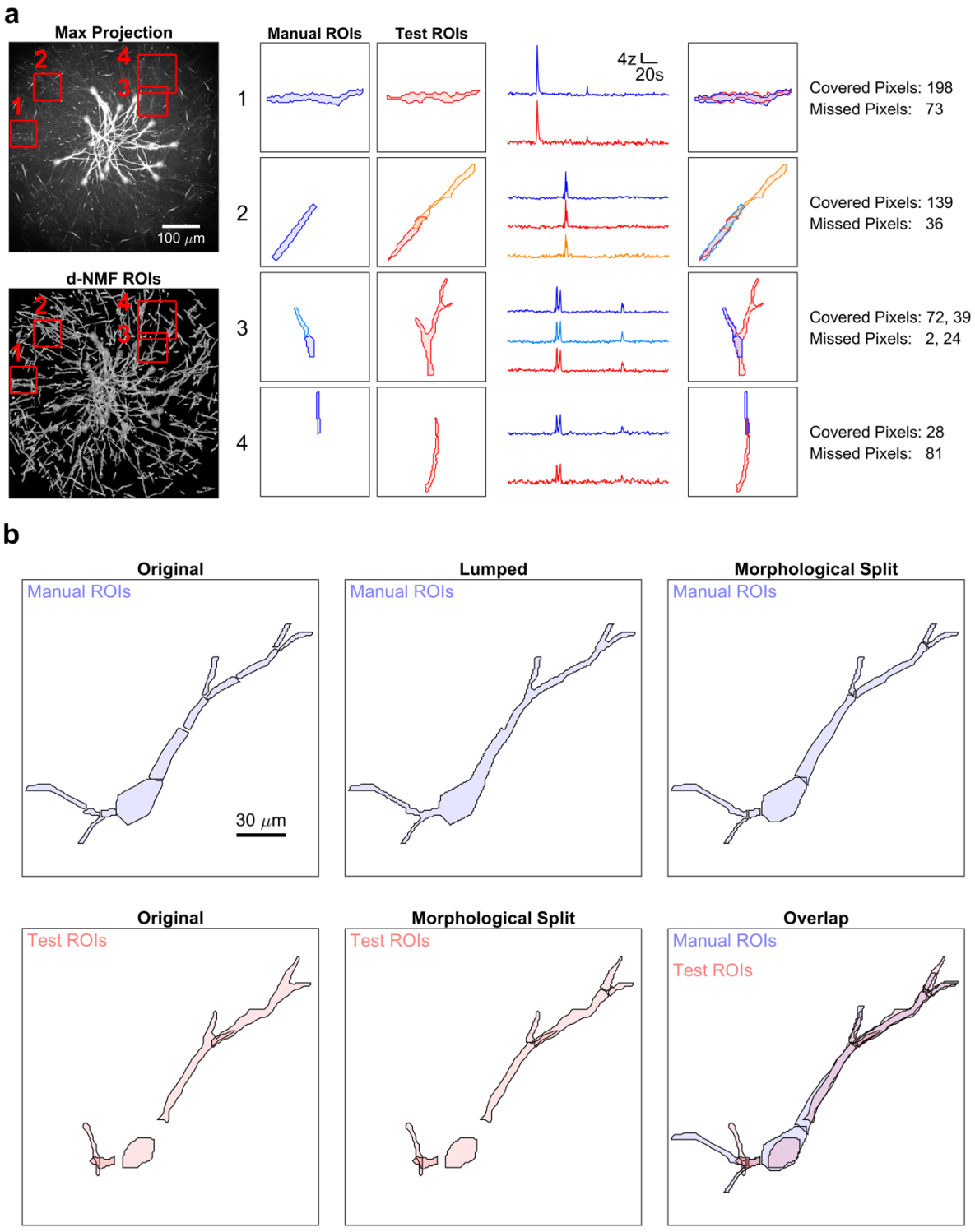

Supplementary Fig. 5 | Evaluating ROI segmentation performance. a, Sample field of view from the synthetic dataset (top) and ROIs identified from d-NMF (bottom). 4 insets show examples of how ROI segmentation performance is evaluated in the synthetic data. Manually-labeled ROIs are indicated in blue shades, and d-NMF identified ROIs (test ROIs) are indicated in red shades. A manual ROI is scored by the proportion of pixels that are covered by any test ROI that has similar activity. **b,** Demonstration of ROI evaluation in the real datasets. Top, the original ROIs drawn by human annotators are grouped by

cell identity to make a “Lumped” ROI, which is then morphologically split at branch points. Bottom, algorithmically defined ROIs are first morphologically split, then the best matches to manual ROIs are identified. Pixels covered by both a manual ROI and test ROI (blue and red) are counted as True Positives. Pixels only in manual ROIs (blue) are False Negatives. Pixels only in Test ROIs (red) are False Positives.

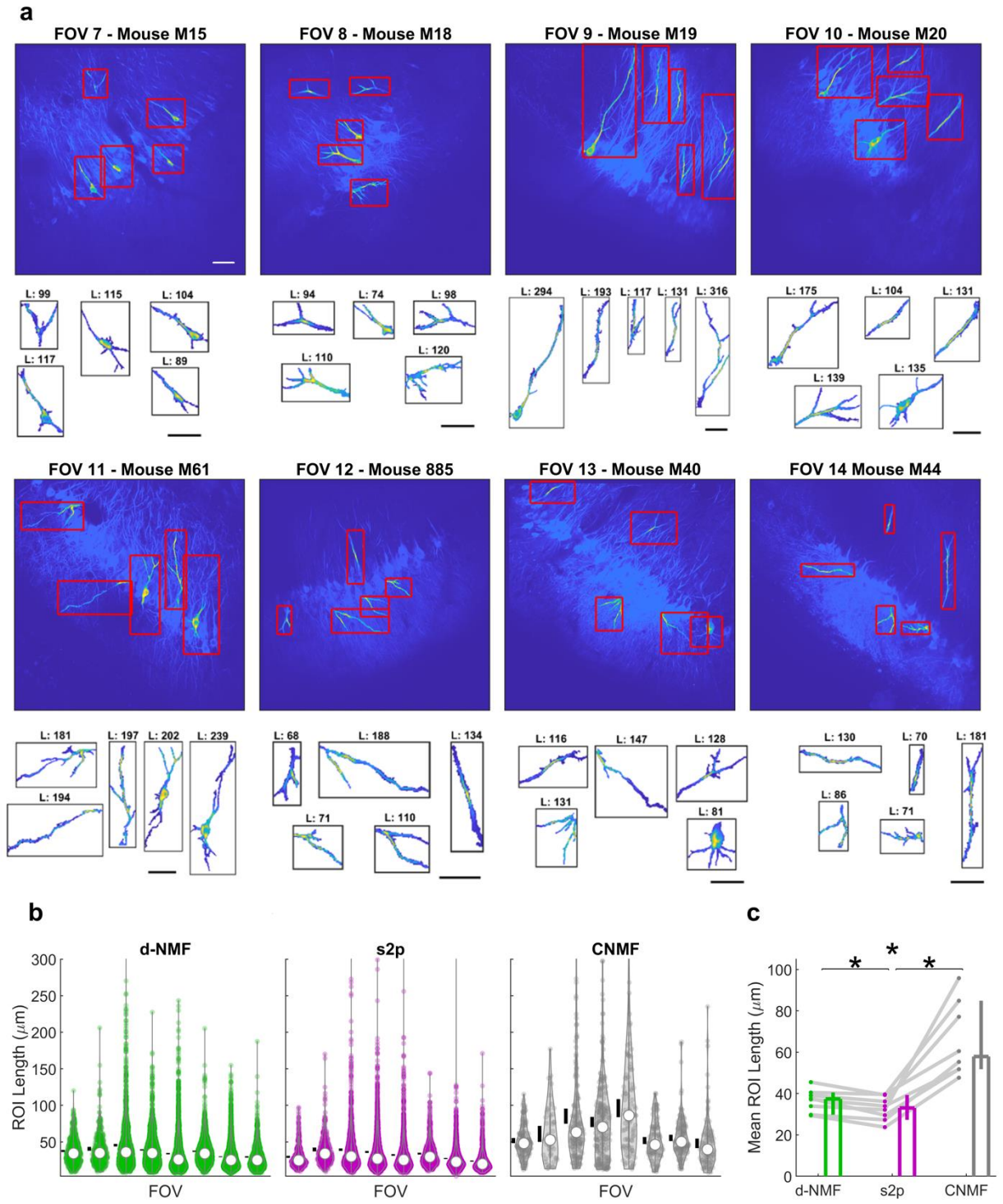

Supplementary Fig. 6 | Illustration of large ROIs detected by d-NMF. a, 8 fields of view from our dense datasets, with 5 sample ROIs each highlighted. Each ROI is labeled with its length L, defined as the longest path (in μm) between any two member pixels. Scale bars denote 50 μm. b, Distributions of ROI lengths for the 8 dense datasets from d-NMF, suite2p, and CNMF. **c**, The median ROI length for d-NMF was 37, [30, 41] μm, significantly larger ($p=7.8\times10^{-3}$, two-sided Wilcoxon signed-rank test) than ROIs obtained from suite 2p (s2p) (33, [27, 39] μm) and significantly smaller ($p=7.8\times10^{-3}$, two-sided Wilcoxon signed-rank test) than those obtained from CNMF (58, [52, 85] μm). CNMF ROIs were also significantly larger ($p=7.8\times10^{-3}$, two-sided Wilcoxon signed-rank test) than suite2p ROIs. *n* = 8 FOVs for all.

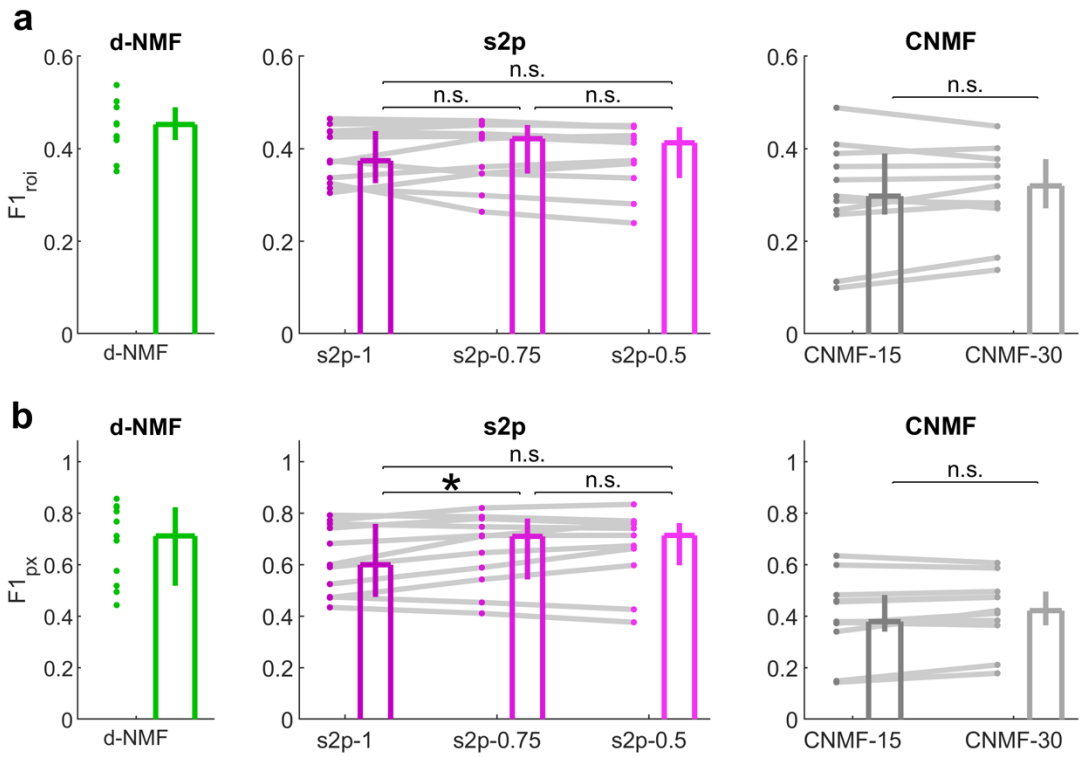

c

Measure	d-NMF	s2p-1	s2p-0.75	s2p-0.5	CNMF-15	CNMF-30
$F1_{roi}$	0.45	0.37	0.42	0.41	0.30	0.32
$F1_{px}$	0.71	0.60	0.71	0.71	0.38	0.42
# ROIs	1190	812	1507	2165	109	164
ROI Size (μm^2)	155.0	108.3	92.0	86.1	473.5	450.2
ROI Length (μm)	37.2	32.1	30.3	25.5	53.4	50.7

Supplementary Fig. 7 | Adjusting thresholds for segmentation methods. a, Left, for reference, the $F1_{roi}$ score for d-NMF (0.45, [0.42, 0.49], *n* = 11 FOVs for all). Middle, suite2p had a small change in $F1_{roi}$ score when the "threshold" parameter was lowered from 1 (0.37, [0.33, 0.44]) to 0.75 (0.42, [0.35, 0.45]) to 0.5 (0.41, 0.34, 0.45]); s2p-1 vs s2p-0.75, p=0.97; s2p-1 vs s2p-0.5, p=0.70; s2p-0.75 vs s2p-0.5, p=0.24, two-sided Wilcoxon signed-rank test). Right, CNMF output was slightly more accurate when the "number of clusters" parameter was changed (CNMF-15, 0.30, [0.26, 0.39]; CNMF-30, 0.32, [0.27, 0.38]; p=0.46, two-sided Wilcoxon signed-rank test). d-NMF vs s2p-0.75: $p=2.0x10^{-3}$; d-NMF vs CNMF-30: $p=9.8x10^{-4}$; s2p-0.75 vs CNMF-30: p=0.014, two-sided Wilcoxon signed-rank test for all. **b,** Same as **a** but for the $F1_{px}$ score. d-NMF: 0.71, [0.52, 0.82]. s2p-1: 0.60, [0.47, 0.76]; s2p-0.75: 0.71, [0.54, 0.78]; s2p-0.5: 0.71, [0.60, 0.76]; s2p-1 vs s2p-0.75, p=0.042; s2p-1 vs s2p-0.5, p=0.15; s2p-0.75 vs s2p-0.5, p=0.52, two-sided Wilcoxon signed-rank test; CNMF-15, 0.38, [0.34, 0.48]; CNMF-30, 0.42, [0.36, 0.50]; p=0.067, two-sided Wilcoxon signed-rank test. d-NMF vs s2p-0.75: p=0.083; d-NMF vs CNMF-30: $p=9.8x10^{-4}$; s2p-0.75 vs CNMF-30: $p=9.8x10^{-4}$, two-sided Wilcoxon signed-rank test for all. **c,** Table of median values of $F1_{roi}$ score, $F1_{px}$ score, number of ROIs, ROI Size, and ROI Length for easy comparison.

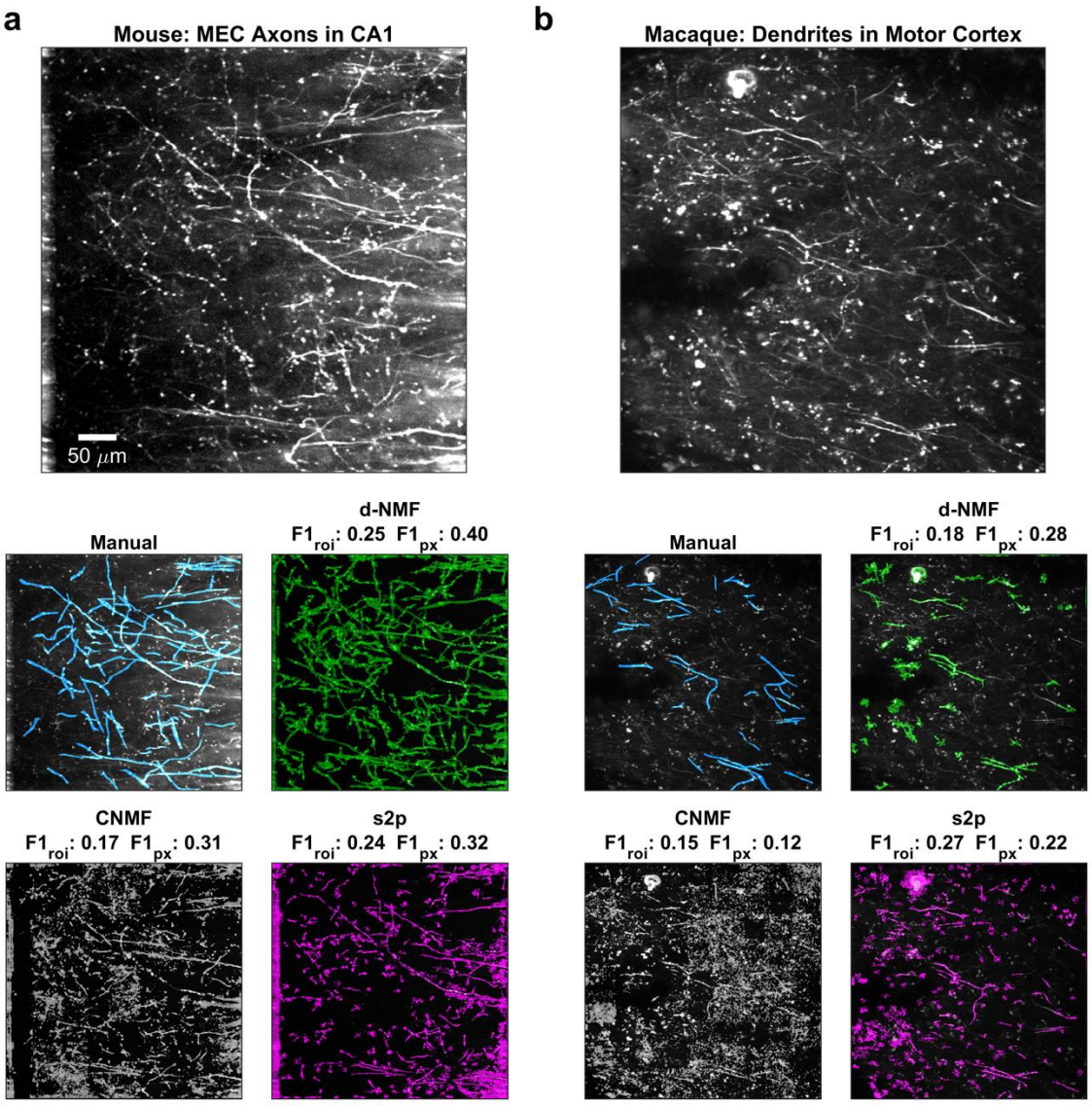

Supplementary Fig. 8 | Application to other datasets. a, Sample field of view with axons from Medial Entorhinal Cortex (MEC) labeled with GCaMP6s, imaged in the Stratum Lacunosum Moleculare of mouse CA1. Top represents the maximum projection image. The panels in the bottom are as in Fig. 4, illustrating ROIs obtained from manual labeling, d-NMF, CNMF, and suite2p. Data reused from Butola et al., Nature Neuroscience 2025 NN-A80353B manuscript with permission from Nature Neuroscience. **b**, Sample field of view with dendrites in macaque motor cortex labeled with GCaMP6f. Data publicly available from Trautmann et al., Nature Communications 2021[36] under Creative Commons Zero v1.0 Universal License (https://spdx.org/licenses/CC0-1.0.html).

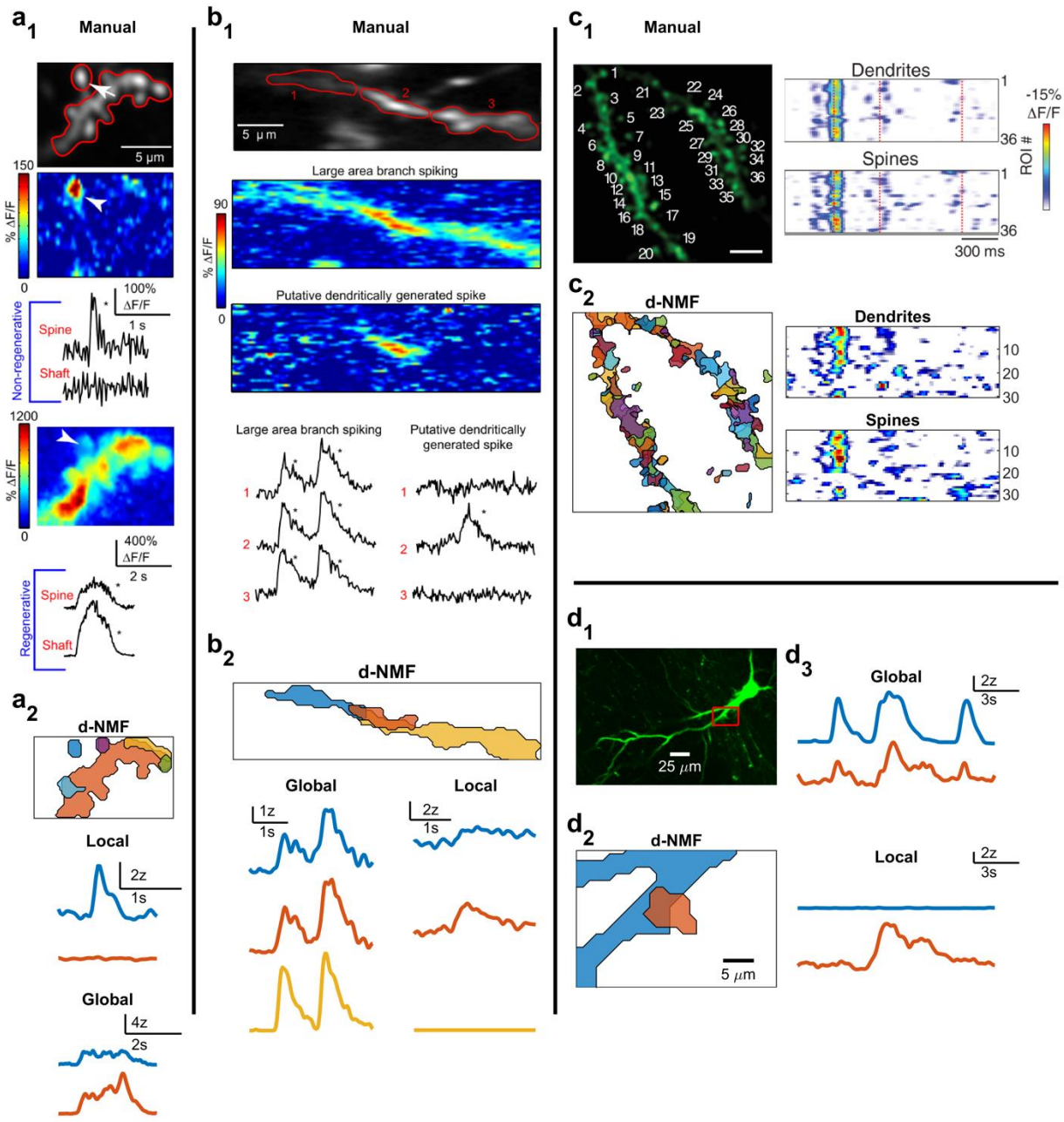

Supplementary Fig. 9 | Fully automatic Identification of localized dendritic activity by d-NMF. a_1, From Sheffield & Dombeck, Nature 2015[21]. Reprinted with permission from Springer Nature. Illustration of a stretch of dendrite of a mouse CA1 pyramidal cell expressing GCaMP6f showing a spine with both localized activity (top) and activity that invades the entire branch (bottom). **a_2,** automatic detection of ROIs on the same dataset using d-NMF identifies the same spine with local (top) and global (bottom) activity. **b_1,** Also from Sheffield & Dombeck, Nature 2015, illustration of a stretch of dendrite of a mouse CA1 pyramidal cell expressing GCaMP6f showing large area branch spiking and a putative locally-generated spike. **b_2,** Automatic ROI detection using d-NMF identifies similar ROIs as those manually-identified and accurately detects global and local activity. **c_1,** From Cornejo et al., Science 2022[37]. Reprinted with permission from AAAS. A dendritic branch of a pyramidal neuron in mouse somatosensory cortex expressing the voltage indicator postASAP, showing localized activity in numbered spines and adjacent dendrites (scale bar = 5 µm). **c_2,** Extracted ROIs (left) and corresponding activity

(right) from d-NMF on the same dataset. $\mathbf{d_1}$, Maximum projection image of a mouse CA3 pyramidal neuron from this study. The red box indicates a region containing a dendritic spine ($\mathbf{d_2}$) automatically identified by d-NMF as having localized activity. $\mathbf{d_3}$, The activity of this spine at times is synchronous with the nearby stretch of dendrite (global, top) but also shows localized activity (local, bottom).

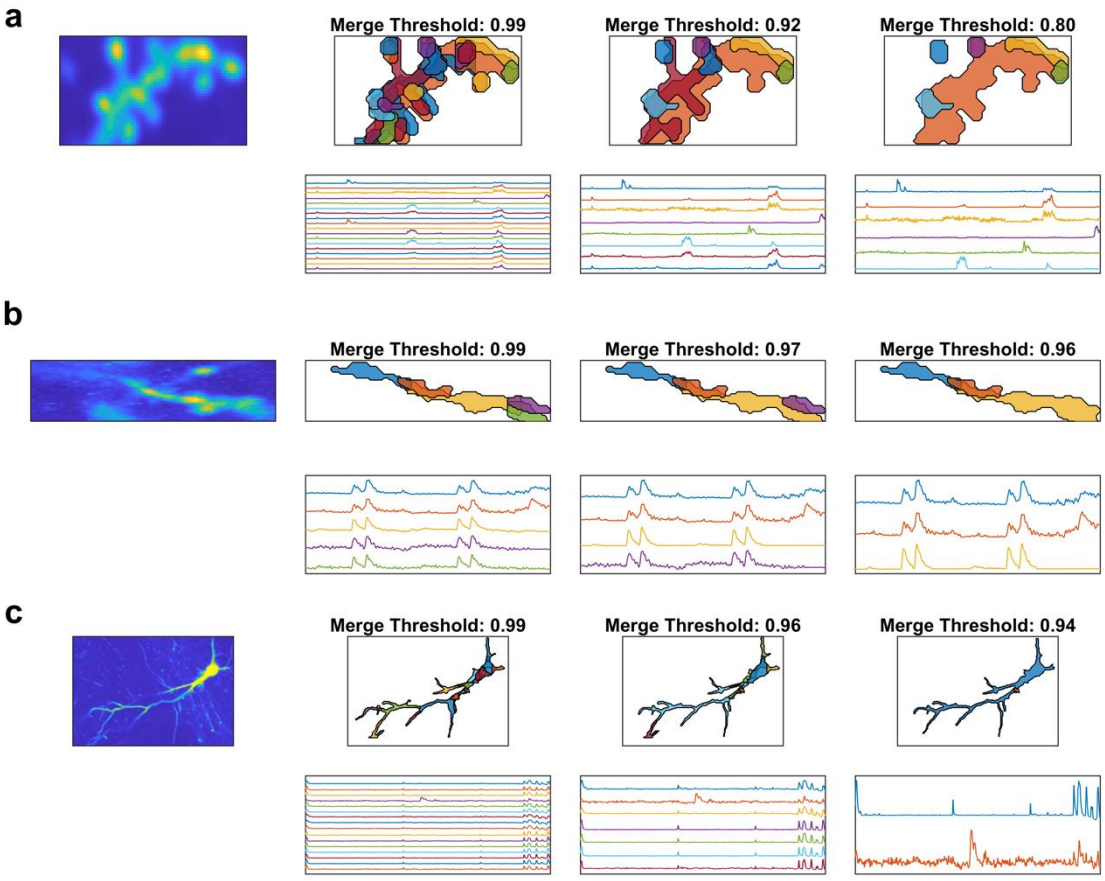

Supplementary Fig. 10 | Exploration of the merging threshold. a, For the dataset in Supplementary Figure 9a, the output of d-NMF is shown for a range of correlation thresholds at which to merge ROIs. The total number of ROIs can vary substantially based on merging threshold, illustrating the importance of choosing the appropriate value for the scientific question at hand. **b,** Same as a but for the dataset in Supplementary Figure 9b. **c,** Same as a but for the dataset in Supplementary Figure 9d.

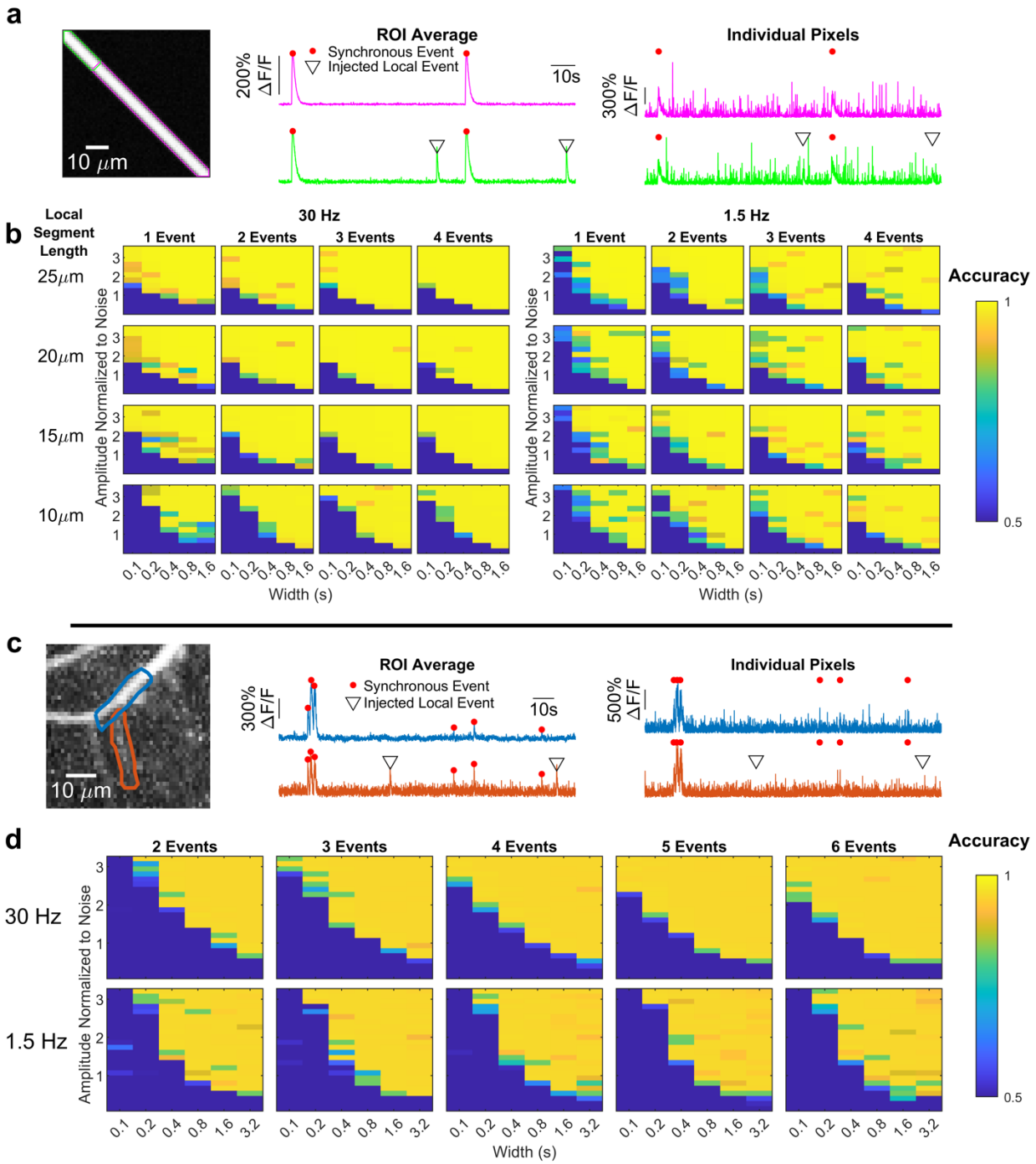

Supplementary Fig. 11 | Exploration of limits of d-NMF in detecting localized dendritic activity. a, Left, Schematic of synthetic data with two ROIs (magenta and green) defined on a dendritic branch showing synchronous events in both ROIs, and local events only in the green ROI. Middle, average ΔF/F of each ROI in a given simulation (2 local events, local length of 20 μm, amplitude of 1.6 x noise level, width of 800 ms). Right, ΔF/F for a randomly-selected pixel of each ROI. Note high signal-to-noise ratio of the mean trace (middle) vs. higher noise for individual pixels. **b**, Accuracy (mean number of ROIs detected across all simulations, divided by 2) of d-NMF in detecting localized activity as a function of width, amplitude, number of events, and segment length for 30 Hz full rate (left) and 1.5 Hz downsampled (right) data. Brief localized events (>1.5 x noise levels) can be detected. **c**, Another synthetic dataset arrangement schematic with localized calcium transients injected into a dendritic branch (red outline) of a real dataset. As in **a-b**, the number, duration, and amplitude of localized events were systematically

varied, and the ability of d-NMF to detect these localized transients was tested. Each combination of parameters was simulated twice. d, As in b, the accuracy of d-NMF in detecting localized activity, defined as the highest spatial correlation of all detected ROIs with the branch ROI outlined in red in **c**. Accuracy is low if the branch ROI is not treated as independent. The maximum accuracy value across 5 simulations is displayed for 30 Hz data (top row) and downsampled 1.5 Hz data (bottom row).

Panel	Parameter	*A*	*τ*	*N*	*L*
b		100:250:3100	[1 2 4 8 16]	[1 2 3 4]	[10 15 20 25]
d		200:200:4800	[1 2 4 8 16 32]	[2 3 4 5 6]	N/A

Supplementary Table 4 | Parameters tested in Supplementary Fig. 11

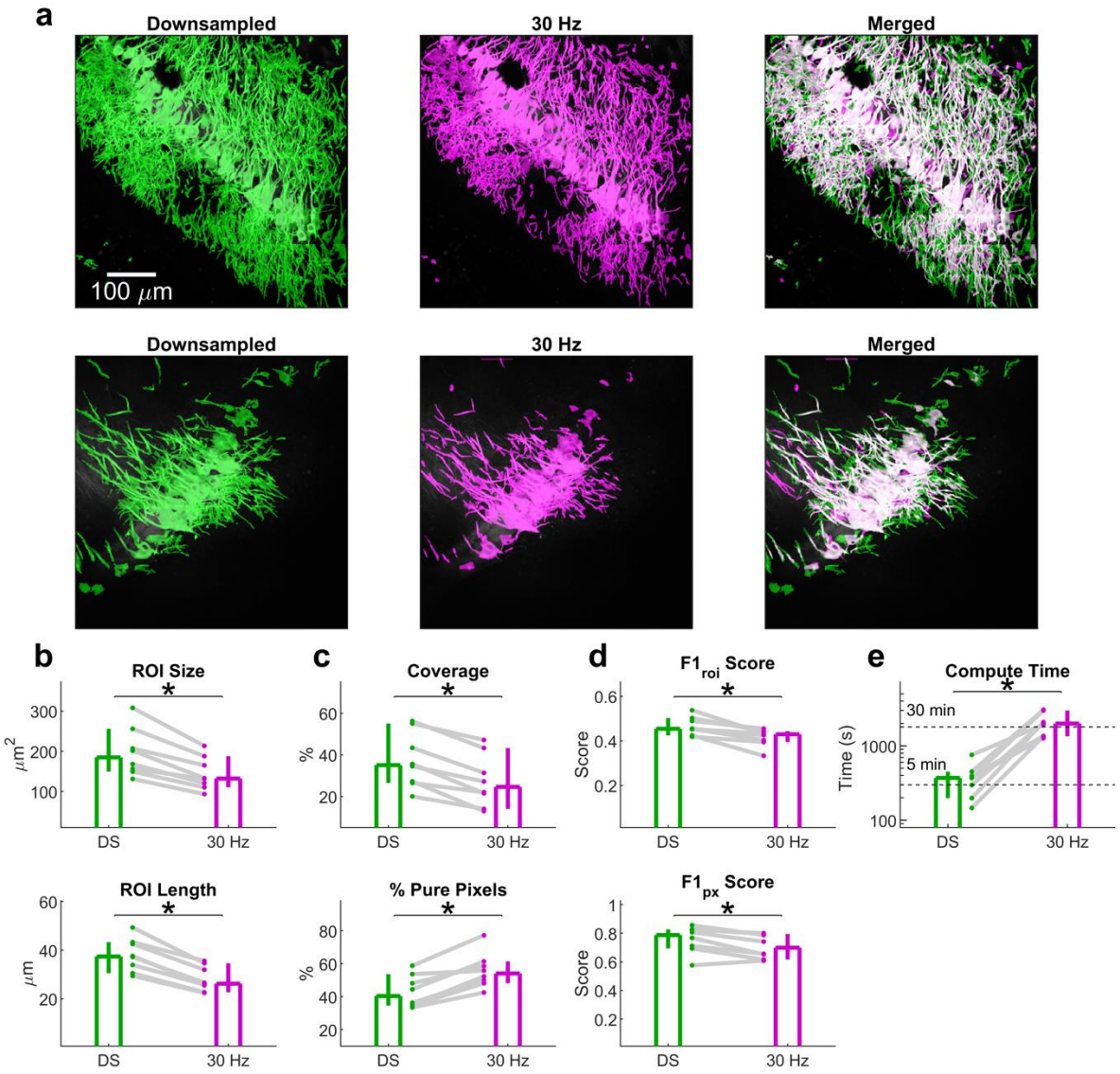

Supplementary Fig. 12 | Similar segmentation of down sampled and non-down sampled data. a, Two example fields of view (top and bottom rows) with ROIs detected from data downsampled to 1.5 Hz (Left, green), original data sampled at 30 Hz (Middle, magenta), and overlay (right). Examples are 2 of 8 FOVs on which the analysis for this figure was performed. **b**, The size of detected ROIs (Top) was smaller when detected using 30 Hz data (130, [110, 190] μm^2) compared to downsampled data (180, [150 260] μm^2, p=0.0078, *n* = 8 FOVs, two-sided Wilcoxon signed-rank test here and throughout), as was the mean ROI length (Bottom, 30 Hz: 26, [23, 35] μm; Downsampled: 37, [31, 43] μm, p=0.0078). **c,** The overall coverage (Top) was also lower using 30 Hz data (25, [14, 43] %) compared to downsampled data (35, [27, 52] %, p=0.0078), and the percentage of pixels belonging to a single ROI (Bottom) was larger in the 30 Hz data (30 Hz: 54, [48, 61] %; Downsampled: 40, [35, 54] %, p=0.0078). **d,** Despite these differences, the $F1_{roi}$ (top) and $F1_{px}$ (bottom) scores compared against manually-labeled data (Top) were not substantially different between the two methods, though the differences were statistically significant ($F1_{roi}$: 30 Hz: 0.43, [0.39, 0.44], DS: 0.45, [0.42, 0.50], p=0.0078; $F1_{px}$: 30 Hz: 0.70, [0.62, 0.80], DS: 0.79, [0.69, 0.83], p=0.039). **e,** Execution time (Bottom) was substantially longer when running d-NMF on raw 30 Hz data (2000, [1300, 3000] seconds) compared to downsampled, 1.5 Hz data (370, [200, 450] seconds).

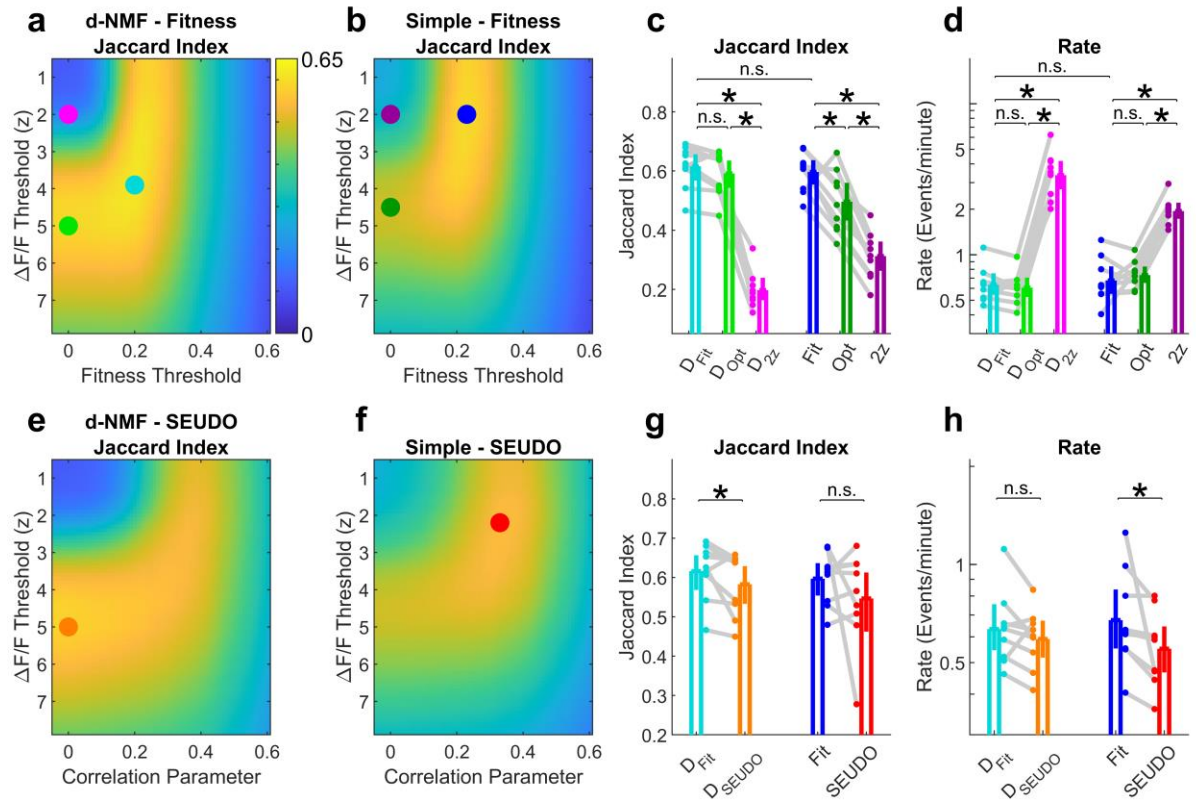

Supplementary Fig. 13 | Event detection for different methods. **a**, Classifier performance for different event classification methods utilizing the de-mixed fluorescence trace and the fitness trace (see Supplementary Table 5 and Methods for details of the classification methods). **b**, Classifier performance for different event classification methods utilizing the simple fluorescence trace (see Methods) and the fitness trace. **c**, D_{Fit} outperformed other methods that did not use the fitness trace. **d**, Same as **c** but for event rate. **e**, Classifier performance when using the SEUDO correlation parameter instead of the Fitness trace on top of the de-mixed fluorescence trace. **f**, Classifier performance when using the SEUDO correlation parameter instead of the Fitness trace on top of the simple fluorescence trace. **g**, Overall classification performance was slightly but significantly higher using the Fitness trace than using SEUDO, both for de-mixed data and simple data. **h**, Detected event rates were not different across the different methods. *n* = 9 sessions for all comparisons. See Supplementary Table 6 for summary statistics.

Name	**2z**	**Opt**	**Fit**	**SEUDO**	**D_{2z}**	**D_{Opt}**	**D_{Fit}**	**D_{SEUDO}**
Primary Trace	Simple ΔF/F	Simple ΔF/F	Simple ΔF/F	Simple ΔF/F	De-mixed ΔF/F	De-mixed ΔF/F	De-mixed ΔF/F	De-mixed ΔF/F
Threshold	2z	Variable	Variable	Variable	2z	Variable	Variable	Variable
Secondary Trace	None	None	Fitness	SEUDO[39]	None	None	Fitness	SEUDO
Threshold	N/A	N/A	Variable	Variable	N/A	N/A	Variable	Variable

Supplementary Table 5 | Table describing details of methods tested in Supplementary Fig. 13. See Methods for further details.

Panel	Measure	Fit	Opt	2z	Fit vs Opt	Fit vs 2z	Opt vs 2z
c	Jaccard, d-NMF	0.62, [0.57, 0.66]	0.59, [0.54, 0.64]	0.19, [0.15, 0.23]	p=0.074	p=0.004	p=0.004
c	Jaccard, Simple	0.60, [0.55, 0.64]	0.50, [0.43, 0.56]	0.31, [0.24, 0.38]	p=0.039	p=0.004	p=0.004
c	D_{Fit} vs Fit: p=0.25						
d	Rate, d-NMF	0.63, [0.55, 0.75]	0.61, [0.52, 0.71]	3.52, [2.22, 4.22]	p=0.20	p=0.004	p=0.004
d	Rate, Simple	0.67, [0.55, 0.84]	0.73, [0.65, 0.83]	1.94, [1.57, 2.13]	p=0.50	p=0.004	p=0.004
d	D_{Fit} vs Fit: p=0.13						
		D_{Fit}	**D_{SEUDO}**	**Comparison**	**Fit**	**SEUDO**	**Comparison**
e	Jaccard	0.62, [0.57, 0.66]	0.58, [0.53, 0.63]	p=0.039	0.60, [0.55, 0.64]	0.55, [0.47, 0.61]	p=0.91
f	Rate	0.63, [0.55, 0.75]	0.59, [0.52, 0.67]	p=0.16	0.67, [0.55, 0.84]	0.55, [0.47, 0.65]	p=0.008

Supplementary Table 6 | Statistics for Supplementary Fig. 13.

Panel	Measure	Apical	Soma	Basal	A vs S	A vs B	S vs B
$\mathbf{e_{top}}$	% Tuned	19, [10, 38]	16, [7, 21]	16 [14, 30]	p=0.31	p=0.95	p=0.55
$\mathbf{e_{bottom}}$	Place field width (cm)	25, [22, 27]	23, [21, 25]	24, [23, 28]	p=0.31	p=0.38	p=1.0
$\mathbf{f_{left}}$	Transient rate (Events/minute)	0.69, [0.51, 1.01]	0.54, [0.45, 0.72]	0.60, [0.55, 0.84]	p=0.016	p=0.38	p=0.039
$\mathbf{f_{right}}$	Correlation with distance	$p=1.1x10^{-8}$		p=0.20			
$\mathbf{g_{left}}$	Transient half-width (ms)	590, [460, 770]	1400, [860, 2400]	590, [400, 870]	p=0.0078	p=0.95	p=0.0078
$\mathbf{g_{right}}$	Correlation with distance	$p=3.3x10^{-9}$		0.48			
$\mathbf{h_{left}}$	Information content	1.87, [1.54, 2.05]	2.07, [1.87, 2.15]	1.93, [1.65, 2.07]	p=0.0078	p=0.64	p=0.0078
$\mathbf{h_{right}}$	Correlation with distance	$p=3.3x10^{-5}$		p=0.55			

Supplementary Table 7 | Statistics for Fig. 6. *n* = 8 sessions for all. Two-sided Wilcoxon signed-rank test used in e_{top}, e_{bottom}, f_{left}, g_{left}, and h_{left}. Two-way ANOVA used for f_{right}, g_{right}, and h_{right}.

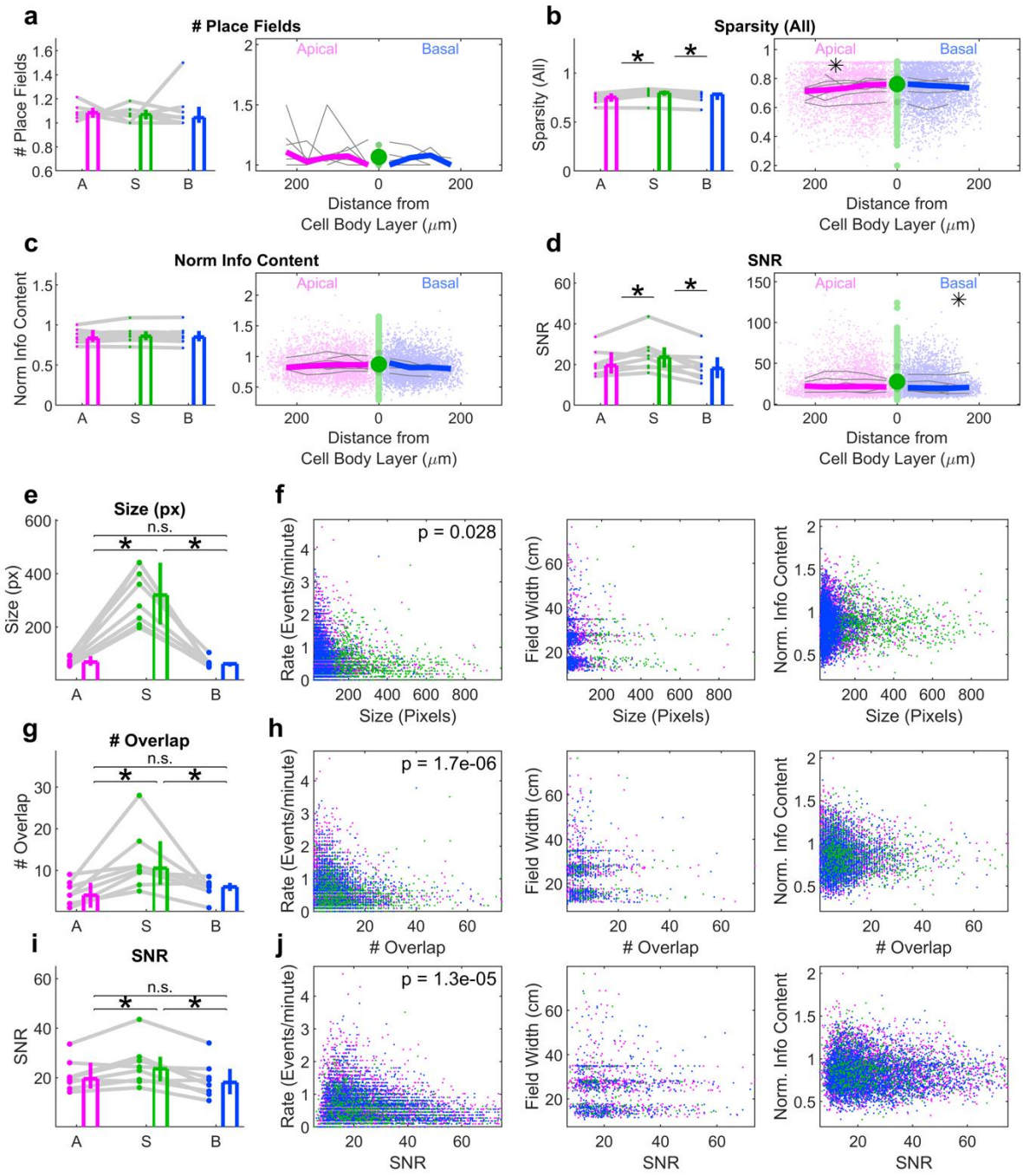

Supplementary Fig. 14 | Additional quantification of basic place tuning properties. a-f, Basic place tuning characteristics did not vary substantially across compartment types. See Supplementary Table 8 for summary statistics. **e**, The mean ROI size (in pixels), was greatest for soma (320, [210, 440] pixels), followed by apical dendrites (68, [54, 84] pixels), then basal dendrites (62, [51, 66] pixels). Apical vs Soma: $p=7.8\times10^{-3}$; Apical vs Basal: p=0.46; Soma vs Basal: $p=7.8\times10^{-3}$ (*n* = 8 FOVs, two-sided Wilcoxon signed-rank test). **f,** Controlling for ROI size, the there was a significant effect of compartment type on event rate (p=0.028, 3-way ANOVA, see Methods), but not field width (p=0.76) or normalized information content (p=0.10). **g**, The mean number of overlapping ROIs was greatest for soma (10.5, [7.25, 17.0]), followed by basal dendrites (6.0, [5.0, 7.0]), then apical dendrites (4.0, [1.0, 7.0]). Apical vs Soma: $p=7.8\times10^{-3}$; Apical vs Basal: p=0.48; Soma vs Basal: p=0.016 (*n* = 8 FOVs, two-sided Wilcoxon signed-rank test). **h,** Controlling for the number of overlapping ROIs, there was a significant effect of compartment type on event rate ($p=1.7\times10^{-6}$, 3-way ANOVA, see Methods), but not field width (p=0.14)

or normalized information content (p=0.22). **i**, The mean signal-to-noise ratio (SNR) was greatest for soma (23.6, [18.5, 28.4]), followed by apical dendrites (19.5, [15.6, 26.0]), then basal dendrites (18.0, [13.3, 23.6]). Apical vs Soma: p=0.039; Apical vs Basal: p=0.078; Soma vs Basal: p=0.016 (*n* = 8 FOVs, two-sided Wilcoxon signed-rank test). **j,** Controlling for the SNR, there was a significant effect of compartment type on event rate ($p=1.3x10^{-5}$, 3-way ANOVA, see Methods), but not field width (p=0.054) or normalized information content (p=0.47).

Panel	Measure	Apical	Soma	Basal	A vs S	A vs B	S vs B
a	# Fields	1.08, [1.04, 1.13]	1.07, [1.00, 1.11]	1.04, [1.00, 1.13]	p=0.46	p=0.74	p=0.81
	Correlation with Distance	p=0.08		p=0.24			
b	Sparsity – All	0.74, [0.70, 0.77]	0.78, [0.74, 0.79]	0.76, [0.71, 0.78]	p=0.0078	p=0.38	p=0.0078
	Correlation with Distance	$p=1.1x10^{-5}$		p=0.77			
c	Norm. Info Content – All	0.85, [0.80, 0.96]	0.87, [0.80, 0.91]	0.86, [0.81, 0.94]	p=1	p=0.84	p=0.74
	Correlation with Distance	p=0.65		p=0.20			
d	SNR	22, [17, 30]	24, [18, 31]	20, [14, 26]	p=0.039	p=0.0078	p=0.016
	Correlation with Distance	p=0.48		p=0.049			

Supplementary Table 8 | Statistics for Supplementary Fig. 14

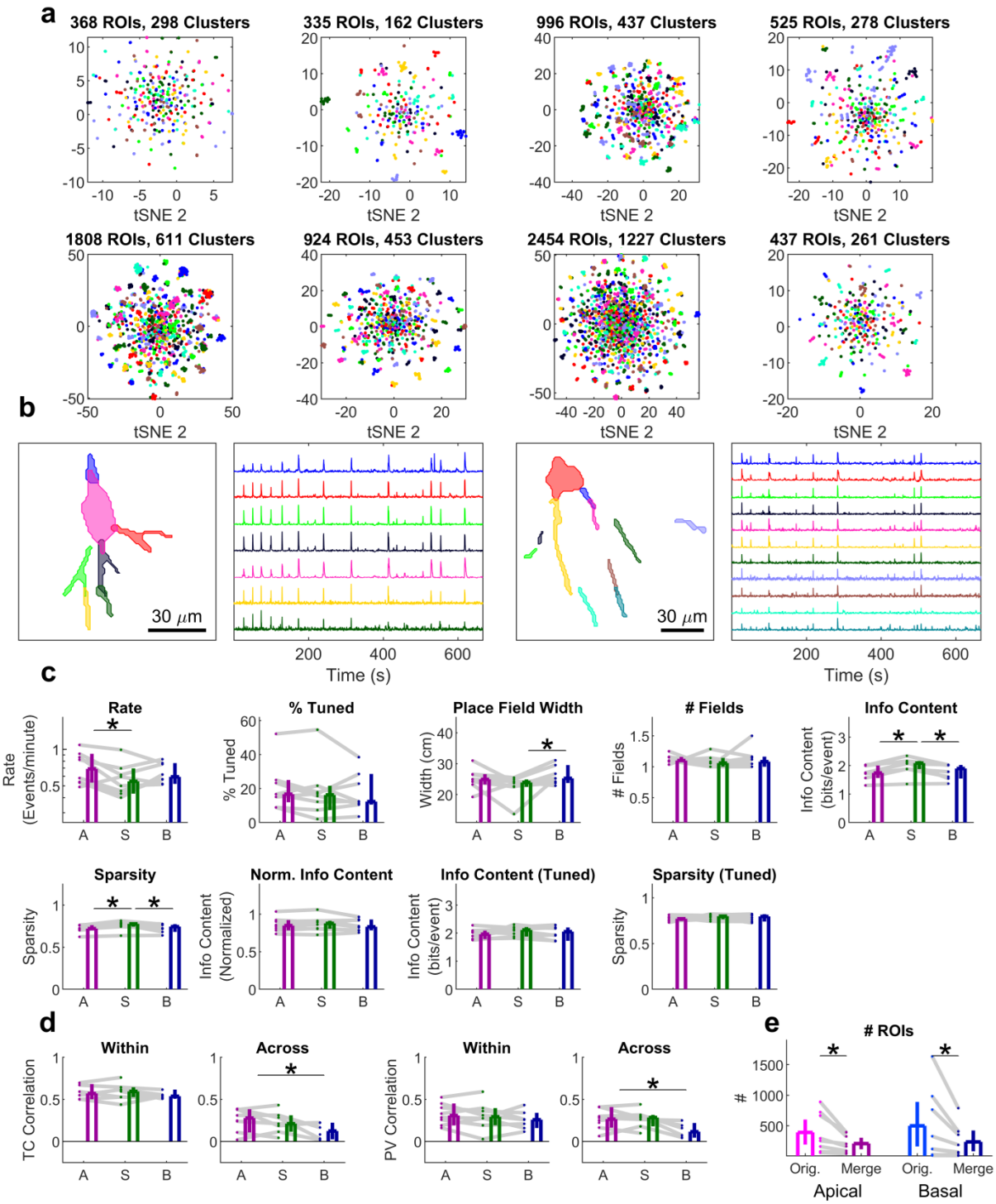

Supplementary Fig. 15 | Merging ROIs with similar activity does not affect scientific conclusions. a, Cluster plots for each FOV in the dense dataset, visualized by t-distributed stochastic neighbor embedding (tSNE). Each dot represents a single ROI, and ROIs are clustered according to their temporal correlation with each other (see Methods). **b,** Two sample cluster groups showing neurons that have been split up into multiple ROIs. **c,** Statistical measures show similar trends and significant differences between the original data and data obtained from merging ROIs with similar activity. See Supplementary Table 9 for summary statistics and compare with Fig. 6 and Supplementary Fig. 14 for values measure on the original, non-merged data. **d,** As in c, but for stability measures. Compare with Fig. 7 for values measured on the original, non-merged data. **e,** The number of apical dendrites in the merged dataset

(210, [120, 310], *n* = 8 FOVs) was ~45% smaller than the number in the original dataset (390, [190, 610]). Similarly, the number of basal dendrites in the merged dataset (240, [80, 430]) was ~50% smaller than the number in the original dataset (500, [160, 900]). *n* = 8 sessions for all comparisons. See Supplementary Table 9 for summary statistics.

Panel	Measure	Apical	Soma	Basal	A vs S	A vs B	S vs B
c	Rate (Orig.)	0.69, [0.51, 1.01]	0.54, [0.45, 0.72]	0.60, [0.55, 0.84]	p=0.016	p=0.38	p=0.039
	Rate (Merge)	0.69, [0.53, 0.92]	0.54, [0.43, 0.70]	0.59, [0.52, 0.77]	p=0.039	p=0.55	p=0.20
c	% Tuned (Orig)	19, [10, 38]	16, [7.1, 21]	16, [14, 30]	p=0.31	p=0.95	p=0.55
	% Tuned (Merge)	17, [8.9, 25]	16, [7.3, 22]	12, [11, 29]	p=0.31	p=0.20	p=1
c	Place Field Width (Orig.)	25, [23, 27]	24, [22, 25]	24, [23, 28]	p=0.25	p=0.95	p=0.74
	Place Field Width (Merge)	25, [23, 27]	24, [22, 25]	25, [24, 39]	p=0.11	p=0.46	p=0.039
c	# Fields (Orig.)	1.09, [1.04, 1.13]	1.07, [1.00, 1.14]	1.05, [1.00, 1.14]	p=0.74	p=0.74	p=0.69
	# Fields (Merge)	1.10, [1.08, 1.16]	1.06, [1.00, 1.14]	1.08, [1.00, 1.16]	p=0.38	p=0.84	p=0.81
c	Info Content – All (Orig.)	1.87, [1.54, 2.05]	2.07, [1.87, 2.15]	1.93, [1.65, 2.07]	p=0.008	p=0.64	p=0.008
	Info Content – All (Merge)	1.74, [1.56, 2.00]	2.09, [1.88, 2.16]	1.90, [1.54, 2.02]	p=0.008	p=0.20	p=0.016
c	Sparsity – All (Orig.)	0.74, [0.70, 0.77]	0.78, [0.74, 0.79]	0.76, [0.71, 0.78]	p=0.008	p=0.38	p=0.008
	Sparsity – All (Merge)	0.72, [0.70, 0.76]	0.78, [0.74, 0.79]	0.74, [0.68, 0.77]	p=0.008	p=0.15	p=0.016
c	Norm. Info Content – All (Orig.)	0.85, [0.80, 0.96]	0.87, [0.80, 0.91]	0.86, [0.81, 0.94]	p=1	p=0.84	p=0.74
	Norm. Info Content – All (Merge)	0.85, [0.78, 0.92]	0.88, [0.80, 0.91]	0.83, [0.78, 0.93]	p=0.38	p=0.64	p=0.31
c	Info Content – Tuned (Orig.)	2.01, [1.79, 2.20]	2.12, [1.88, 2.19]	2.15, [1.88, 2.33]	p=0.74	p=0.25	p=0.31
	Info Content – Tuned (Merge)	1.96, [1.79, 2.09]	2.11, [1.88, 2.22]	2.05, [1.73, 2.20]	p=0.15	p=0.46	p=0.25
c	Sparsity – Tuned (Orig.)	0.78, [0.74, 0.81]	0.80, [0.76, 0.82]	0.80, [0.77, 0.83]	p=0.31	p=0.2	p=0.31
	Sparsity – Tuned (Merge)	0.77, [0.75, 0.79]	0.80, [0.76, 0.81]	0.80, [0.74, 0.82]	p=0.20	p=0.46	p=0.74
d	TC Correlation – Within (Orig.)	0.62, [0.52, 0.69]	0.59, [0.52, 0.66]	0.56, [0.53, 0.63]	p=0.69	p=1	p=0.62
	TC Correlation – Within (Merge)	0.57, [0.50, 0.68]	0.59, [0.53, 0.64]	0.54, [0.51, 0.62]	p=1	p=0.88	p=0.62
d	TC Correlation – Across (Orig.)	0.32, [0.13, 0.39]	0.20, [0.11, 0.32]	0.14, [0.03, 0.23]	p=0.16	p=0.031	p=0.31
	TC Correlation – Across (Merge)	0.28, [0.11, 0.38]	0.21, [0.11, 0.31]	0.12, [0.03, 0.22]	p=0.47	p=0.031	p=0.31
d	PV Correlation – Within (Orig.)	0.35, [0.20, 0.44]	0.30, [0.20, 0.40]	0.29, [0.16, 0.37]	p=0.38	p=0.023	p=0.64
	PV Correlation – Within (Merge)	0.31, [0.19, 0.45]	0.29, [0.19, 0.40]	0.26, [0.16, 0.34]	p=0.64	p=0.22	p=0.81

d	PV Correlation – Across (Orig.)	0.29, [0.18, 0.38]	0.28, [0.16, 0.32]	0.12, [0.02, 0.24]	p=0.47	p=0.031	p=0.12
	PV Correlation – Across (Merge)	0.26, [0.16, 0.41]	0.28, [0.18, 0.32]	0.12, [0.04, 0.22]	p=1	p=0.031	p=0.062
Panel	**Measure**	**Original**		**Merged**		**Comparison**	
e	# ROIs (Apical)	390, [190, 610]		210, [120, 310]		p=0.0078	
	# ROIs (Basal)	500, [160, 900]		240, [80, 430]		p=0.0078	

Supplementary Table 9 | Statistics for Supplementary Fig. 15.

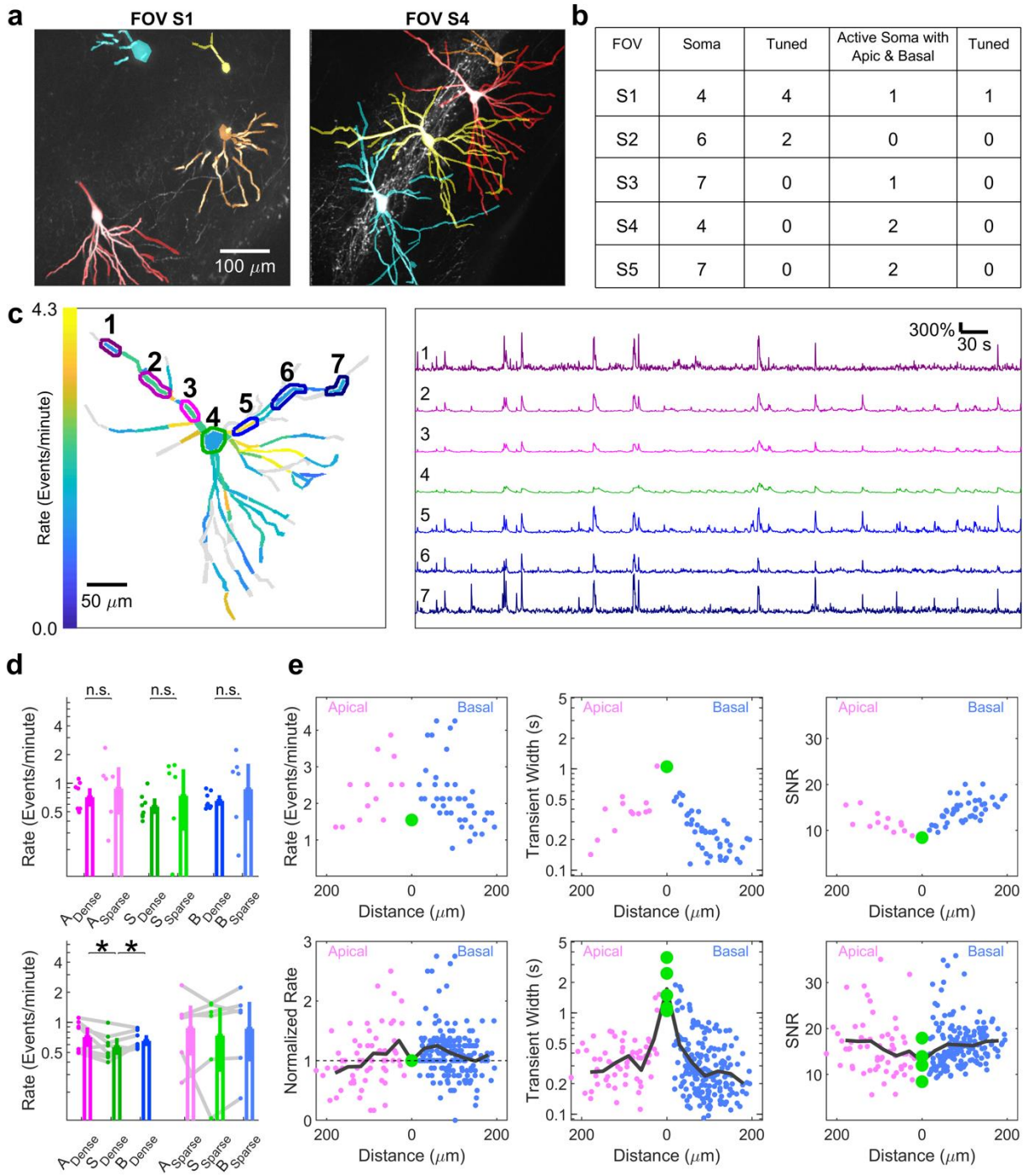

FOV	Soma	Tuned	Active Soma with Apic & Basal	Tuned
S1	4	4	1	1
S2	6	2	0	0
S3	7	0	1	0
S4	4	0	2	0
S5	7	0	2	0

Supplementary Fig. 16 | Sparsely labeled data reproduces dense dataset trends. a. Maximum intensity projections of two sample fields of view from sparsely labeled mice, with neuron skeletons overlaid in different colors. **b.** Table showing the number of soma obtained in each field of view. **c.** Left, sample neuron (red highlighted neuron from FOV S4) pseudocolored with the event rate in each compartment. 7 sample ROIs are indicated with outlines. Right, fluorescence traces for the 7 indicated ROIs. Note there are more calcium transients the closer the ROI is to the soma (ROI 4, green). Activity is plotted as ΔS/S, where S is the ratio of green GCaMP to red tdTomato (see Methods). **d.** Top, overall activity rates were comparable between dense and sparse data for apical dendrites (Dense: 0.71, [0.57, 0.88]; Sparse: 0.88, [0.47, 1.48], p=0.35, two-sided Wilcoxon rank-sum test), soma (Dense: 0.57, [0.47, 0.70]; Sparse: 0.74, [0.32, 1.40], p=0.28, two-sided Wilcoxon rank-sum test), and basal dendrites (Dense: 0.65, [0.58, 0.74]; Sparse: 0.86, [0.40, 1.60], p=0.35, two-sided Wilcoxon rank-sum test). Bottom, apical and basal

dendrites had significantly higher rates than soma in the dense data. This trend was observed in the sparse data as well (Apical vs Soma, p=1; Apical vs Basal, p=0.56; Soma vs Basal, p=0.22, two-sided Wilcoxon signed-rank test for all). Data here are presented as mean and 95% confidence interval of the mean rather than median because there are only 6 data points in the sparse dataset, making the median a brittle measure. **e.** Top, activity rate, transient width, and signal-to-noise ratio (SNR) as a function of distance from the soma for the example neuron in **c.** Bottom, aggregated normalized rates, transient widths, and SNR for all recorded neurons in the sparse datasets. Black line indicates the average in 30 μm bins.

Panel	Measure	Apical	Soma	Basal	A vs S	A vs B	S vs B
d	Tuning curve correlation	0.42, [0.34, 0.49]; *n* = 111	0.28, [0.17, 0.39]; *n* = 54	0.25, [0.14, 0.36]; *n* = 61	N/A	N/A	N/A
$\mathbf{f_{left}}$	Within-day tuning curve correlation	0.62, [0.52, 0.69]	0.59, [0.52, 0.66]	0.56, [0.53, 0.63]	p=0.69	p=1.0	p=0.63
$\mathbf{f_{right}}$	Across-day tuning curve correlation	0.32, [0.13, 0.39]	0.20, [0.11, 0.32]	0.14, [0.03, 0.23]	p=0.16	p=0.031	p=0.31
$\mathbf{g_{left}}$	Within-day population vector correlation	0.35, [0.20, 0.44]	0.30, [0.20, 0.40]	0.29, [0.16, 0.37]	p=0.38	p=0.023	p=0.64
$\mathbf{g_{right}}$	Across-day population vector correlation	0.29, [0.18, 0.38]	0.28, [0.16, 0.32]	0.12, [0.02, 0.24]	p=0.47	p=0.031	p=0.13

Supplementary Table 10 | Statistics for Fig. 7. n = 8 sessions for f_{left}, f_{right}, g_{left}, and g_{right}. Two-sided Wilcoxon signed-rank test used in f_{left}, f_{right}, g_{left}, and g_{right}. No statistical comparisons were made in panel d.

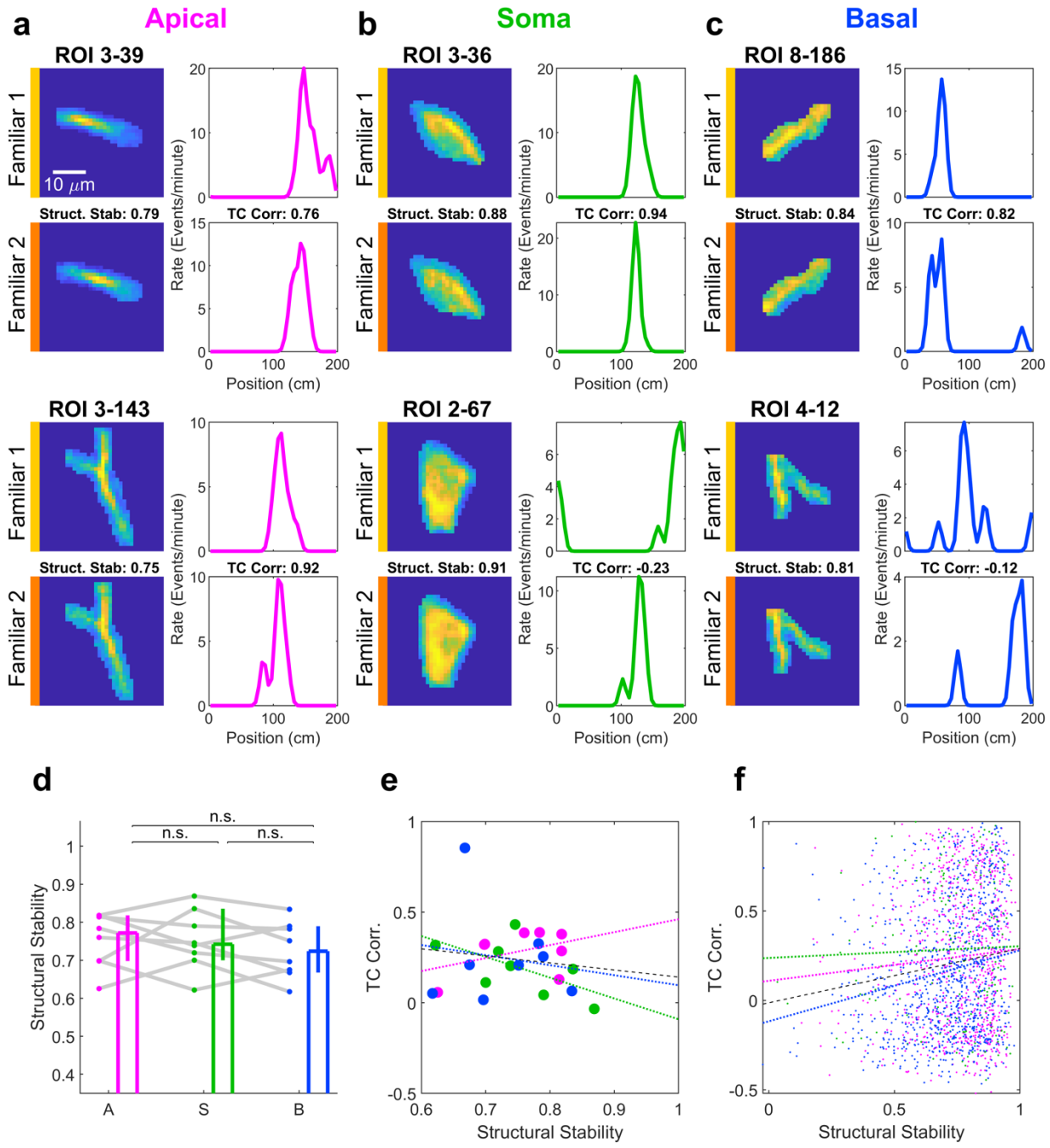

Supplementary Fig. 17 | Stability of FOV and ROIs across days. a, Two example apical dendrite ROIs tracked across consecutive days: Familiar 1 (top, yellow bar) and Familiar 2 (bottom, orange bar). The surface plots on the left indicate the mean value of the ROI across the frames with detected calcium transients. Structural stability is defined as the correlation coefficient between these two surface plots. The plots on the right indicate the rate map of the given ROI as a function of position. Tuning Curve (TC) correlation is defined as the correlation coefficient between these two rate maps. **b**, Same as **a** but for two example somatic ROIs. Note the second example has high structural stability but an entirely different tuning curve between the two days. **c**, Same as **a** but for two example basal dendrite ROIs. As in **b**, note the second example has high structural stability but low TC correlation. **d**, Structural stability was relatively high and not statistically significantly different across compartment types (Apical: 0.77, [0.70, 0.82]; Soma: 0.74, [0.70 0.84]; Basal: 0.72, [0.67, 0.79]; Apical vs Soma: p=0.84; Apical vs Basal:

p=0.20; Soma vs Basal: p=0.25, two-sided Wilcoxon signed-rank test, *n* = 8 FOVs for all). **e**, There was no systematic relationship between structural stability and across-day TC correlation when averaged within mice (Effect of structural stability on TC corr: p=0.57; Effect of interaction between compartment type and structural stability: p=0.42, 2-way ANOVA, *n* = 8 sessions x 3 compartment types). **f**, There was no systematic relationship between structural stability and across-day TC correlation when datapoints were considered independent (Effect of structural stability on TC corr: $p=9.3x10^{-4}$; Effect of interaction between compartment type and structural stability: p=0.42, 3-way ANOVA, *n* = 1983 ROIs across 8 sessions).

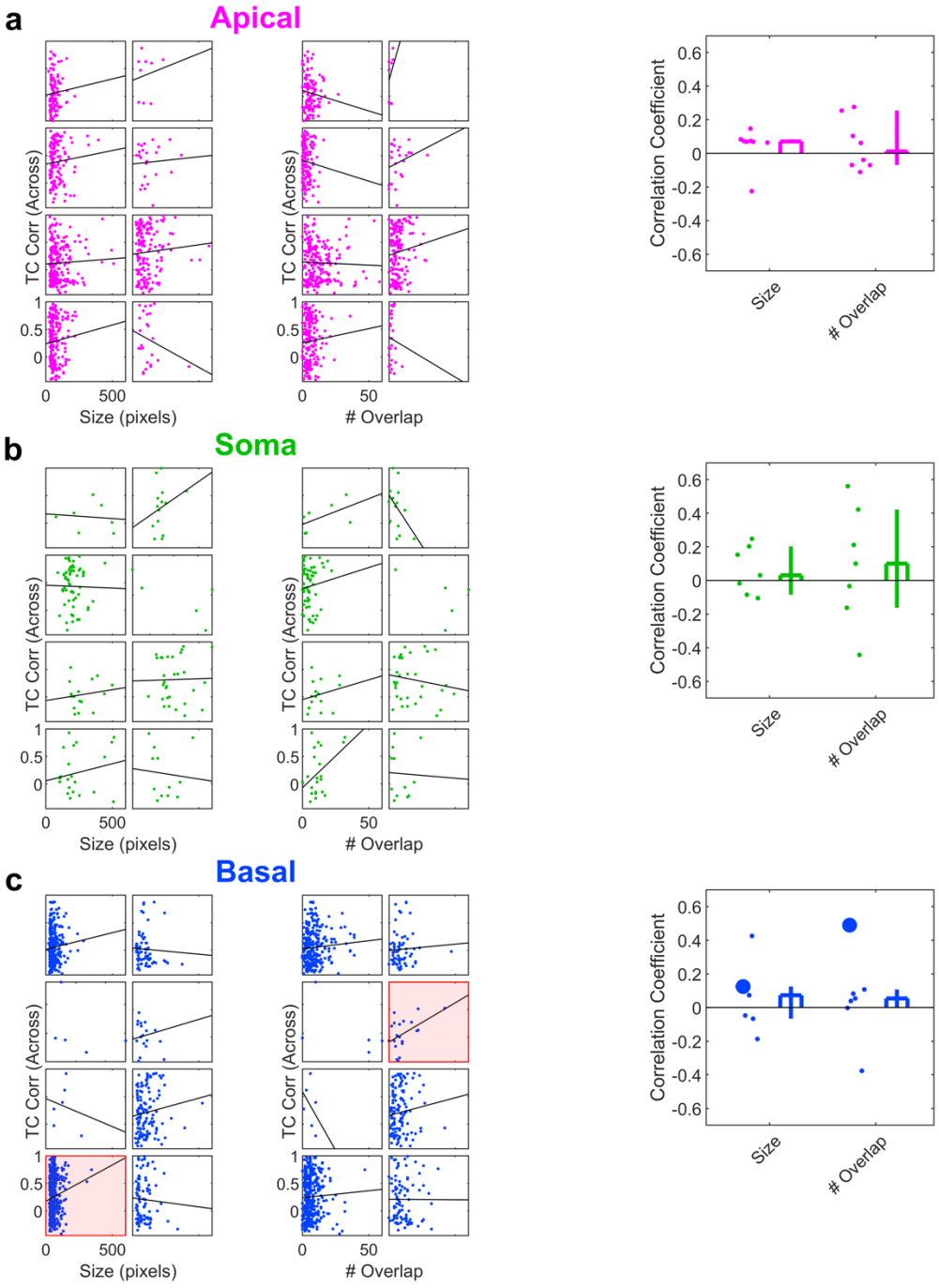

Supplementary Fig. 18 | Relationship between size and overlap number with across-day tuning curve correlation. a, Left, scatter plots relating Apical Dendrite ROI overlap count and ROI size to across-day Tuning Curve correlation. Each box contains data from an individual mouse. Datasets with a statistically significant correlation are highlighted in red. Datasets with fewer than 6 ROIs were excluded from analysis and do not have a correlation line drawn. Right, the distribution of correlation coefficients across all mice. Statistically significant correlations in individual mice are marked with large dots. Size: 0.07, [0.06, 0.08]; # Overlap: 0.01, [-0.07, 0.25]. *n* = 8 FOVs for all. **b**, Same as **a** but for somatic ROIs. Size: 0.03, [-0.08, 0.20], *n* = 7 FOVs; # Overlap: 0.10, [-0.16, 0.42], n=7 FOVs. **c**, Same as **a** but for basal dendrite ROIs. Size: 0.07, [-0.07, 0.12], *n* = 7 FOVs; # Overlap: 0.05, [-0.00, 0.11], *n* = 7 FOVs.